Designing exceptional-point-based graphs yielding topologically guaranteed quantum search

Quancheng Liu [1,*] David A. Kessler,[2] and Eli Barkai[1]

[1]*Department of Physics, Institute of Nanotechnology and Advanced Materials, Bar-Ilan University, Ramat-Gan 52900, Israel*

[2]*Department of Physics, Bar-Ilan University, Ramat-Gan 52900, Israel*

(Received 9 February 2022; accepted 24 April 2023; published 31 May 2023)

Quantum walks underlie an important class of quantum computing algorithms, and represent promising approaches in various simulations and practical applications. Here we design stroboscopically monitored quantum walks and their subsequent graphs that can naturally boost target searches. We show how to construct walks with the property that all the eigenvalues of the non-Hermitian survival operator, describing the mixed effects of unitary dynamics and the back-action of measurement, coalesce to zero, corresponding to an exceptional point whose degree is the size of the system. Generally, the resulting search is guaranteed to succeed in a bounded time for any initial condition, which is faster than classical random walks or quantum walks on typical graphs. We then show how this efficient quantum search is related to a quantized topological winding number and further discuss the connection of the problem to an effective massless Dirac particle.

DOI: 10.1103/PhysRevResearch.5.023141

I. INTRODUCTION

Quantum walks [1,2], the quantum analog of the well-known classical random walks, have attracted increasing attention due to their importance both in fundamental physics and applications for quantum information processing [3]. Taking advantage of coherent superposition and interference, the quantum walk in many respects is superior to its classical counterpart and finds applications in quantum algorithms [4,5], universal quantum computation [6,7], quantum simulation [2,8], and biochemical processes [9,10]. One main challenge of the quantum walk is to maximize the detection probability on a predetermined target state $|\psi_{\rm d}\rangle$ given some initial state $|\psi_0\rangle$ [11,12]. With unitary evolution, nearly perfect quantum search with detection probability approaching unity was found in several graphs for some special initial states at some particular time t, including a glued binary tree [12], a hypercube, and high-dimensional lattices [11], while typical systems fall far from this limit. In a broad sense, the transfer of a known initial state to another state is called quantum state transfer [13–15]. *For instance*, Kostak *et al.* designed permutation operations that propagate the system from one specific node of the graph to another at a predetermined time t [16], obtaining perfect state transfer. However, if one does not know what the initial condition is, as is typical in many search problems, we cannot fully rely on the quantum state transfer or one-shot measurement quantum walks. Therefore, we herein design special graphs and measurement protocols, with the aim to achieve what we call a guaranteed search. Namely, the quantum walker should be successfully detected in a bounded time for any initial condition. We describe how to construct such quantum graphs and corresponding measurement strategies. We further investigate whether these measurements, that destroy the unitary evolution, are either harmful or useful for the search, and in what sense.

Our work is motivated by the state-of-the-art technology advances in experiments [17] that allow clever engineering of Hamiltonians with superconducting circuits [18], waveguide arrays [19–24], trapped ions [25,26], and arrays of neutral atoms generated either in an optical cavity [27] or via optical tweezers [28]. For instance, using photons carrying information between atomic spins, programmable nonlocal interactions in an array of atomic ensembles are realized in an optical cavity [27]. These advances allow us to consider the option of constructing a device with nontrivial matrix elements of the Hamiltonian and thus design special types of graphs to speed up the quantum search.

We find that the designed quantum graphs (see Fig. 1), together with the stroboscopic search protocol, have remarkable search capabilities, either with or without control of the initial state. The ability to search an unknown initial state, i.e., a black-box initial state, is a significant step forward, in contrast to previous works that considered quantum walks that start from a uniform or specific localized initial state. Physically, one of the features of efficient quantum search we find here is that it is intimately related to the study of exceptional points. The latter are degenerate eigenvalues of the non-Hermitian operators that are studied, for example, in optics and laser physics [29–32], and topological phases [33–36], and are fundamentally related to parity-time symmetry breaking [37–39]. Here, we design graphs and a search protocol with an exceptional point of unusually high degeneracy, namely, the size of the entire Hilbert space, which can be made as large as we wish. We highlight the idea that exceptional search is found when all the eigenvalues of the survival operator,

*qcliu.ac@gmail.com

Published by the American Physical Society under the terms of the Creative Commons Attribution 4.0 International license. Further distribution of this work must maintain attribution to the author(s) and the published article's title, journal citation, and DOI.

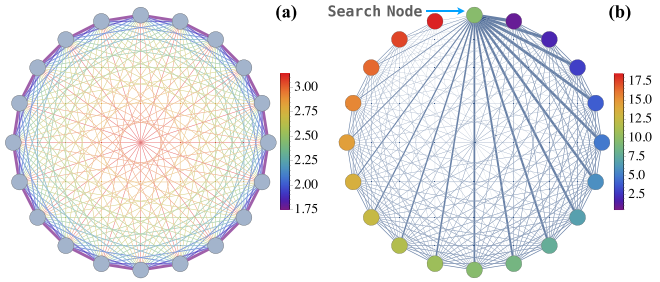

FIG. 1. Designed quantum graphs. Schematic presentation of the crawl graph (a) and funnel model (b). Here $N = 20$. The thickness of the connecting line represents the strength of the matrix element connecting two nodes [(a) and (b)]. The colors represent the phases of the hopping rates (a). In (b) we utilize colors to represent the magnitude of the onsite energies, whose matrix elements are real (see details in Appendix C). The search on both graphs is guaranteed to succeed within a bounded time, for any initial condition.

defined below, coalesce to zero, creating a large degeneracy. We then explore the topology of the model at the exceptional point and show that efficient quantum search is related to the quantization of certain topological winding numbers. Towards the end of the paper, we show how the search problem and the corresponding degeneracy of the exceptional points and the topological property are related to an effective massless Dirac particle, though all along we use Schrödinger dynamics. We also show how our search strategies are related to quantum state transfer.

II. STROBOSCOPIC SEARCH PROTOCOL AND *N*th-ORDER EXCEPTIONAL POINT

To perform efficient quantum walks, we use the strategy of stroboscopic measurements, which as we show later can be made into an efficient tool. In the stroboscopic protocol, the quantum walker starts from an unknown initial state $|\psi_0\rangle$ and evolves unitarily according to the graph Hamiltonian H. We projectively measure the system at times $\tau, 2\tau, \ldots,$ at each measurement asking if the system is found at its target, namely, at $|\psi_d\rangle$. The search target can be a localized node on the graph; however, in general this is not a requirement. This yields a string of $n-1$ successive "No's" followed by a "Yes" from the nth measurement. Once we record a Yes, the system is at the target state $|\psi_d\rangle$ and, in that sense, we have a successful quantum search. The time $n\tau$ is the search time of the target state $|\psi_d\rangle$, which is clearly a random variable whose statistical properties ultimately depend on the initial state of the system $|\psi_0\rangle$, the unitary evolution between measurements, and the choice of τ.

Let F_n be the probability of detecting the system in state $|\psi_d\rangle$ for the first time at $n\tau$. Then the total search probability of finding the quantum walker on the target state is $P_{\rm det} = \sum_{n=1}^{\infty} F_n$. If $P_{\rm det} = 1$ the mean search time is $\langle t\rangle = \tau \sum_{n=1}^{\infty} nF_n$. The search probability F_n is given in terms of the amplitudes ϕ_n of first detection, namely, $F_n = |\phi_n|^2$ with [40–45]

$$\phi_n = \langle\psi_d|U(\tau)\mathcal{S}^{n-1}(\tau)|\psi_{\rm in}\rangle, \tag{1}$$

where the survival operator is $\mathcal{S}(\tau) = (1 - |\psi_d\rangle\langle\psi_d|)U(\tau)$, with $U(\tau) = \exp(-iH\tau)$ and $\hbar = 1$. Here the back-action of the first $n-1$ repeated measurements is to repeatedly project out the amplitude of the target state $|\psi_d\rangle$. In Eq. (1) we have used the basic postulates of quantum theory with the projection $1 - |\psi_d\rangle\langle\psi_d|$.

As usual with these types of problems, the eigenvalues of the non-Hermitian operator $\mathcal{S}(\tau)$ are essential for the characterization of the process. The eigenvalues of $\mathcal{S}(\tau)$, denoted ξ, are all on or inside the unit circle $|\xi| \leqslant 1$, and the eigenvalues with $|\xi| = 1$ correspond to dark states [44,46,47]. *Our goal* is to find $U(\tau)$ and the corresponding H so that *all* the eigenvalues of $\mathcal{S}(\tau)$ are equal to zero. Intuitively, if all the eigenvalues are very small, the decay of F_n is expected to be fast and the quantum search time will be minimized. It is also clear that if we find such H, with all the eigenvalues ξ coalescing to the value $\xi = 0$, then we have engineered a method that yields a survival operator with a Nth-order exceptional point, N being the size of the system.

The eigenvalues ξ are given implicitly by

$$\det|\xi - \mathcal{S}(\tau)| = \xi \det|\xi - U(\tau)|\langle\psi_d|\frac{1}{\xi - U(\tau)}|\psi_d\rangle = 0, \tag{2}$$

where we have used the matrix determinant lemma (see Appendix A). Clearly, the system always has at least one solution $\xi = 0$. Let $H|E_k\rangle = E_k|E_k\rangle$ where $k = 0, \ldots, N-1$ and as usual we may expand $|\psi_d\rangle = \sum_{k=0}^{N-1}\langle E_k|\psi_d\rangle|E_k\rangle$, and then

$$\langle\psi_d|\frac{1}{\xi - U(\tau)}|\psi_d\rangle = \sum_{k=0}^{N-1}\frac{p_k}{\xi - \exp(-iE_k\tau)} \tag{3}$$

with $\det|\xi - U(\tau)| = \prod_{k=0}^{N-1}[\xi - \exp(-iE_k\tau)]$. Here $p_k = |\langle E_k|\psi_d\rangle|^2$ is the square of the overlap between the energy state $|E_k\rangle$ and the detected state. Our first requirement is that the system is such that $p_k \neq 0$ for all the energy states $|E_k\rangle$, and that there is no degeneracy, i.e., $\exp(-iE_k\tau) \neq \exp(-iE_m\tau)$ for any choice of $m \neq k$. Physically this demand means that we exclude dark states so that $|\xi| < 1$ and hence the eigenvalues satisfy $\det|\xi - U(\tau)| \neq 0$. Using Eqs. (2) and (3) it is not difficult to show that the eigenvalue problem reduces to finding the solution of

$$\xi\sum_{k=0}^{N-1}\frac{p_k}{\xi - \exp(-iE_k\tau)} = 0. \tag{4}$$

We now engineer the system in such a way that the only solution is the degenerate solution with $\xi = 0$. As we will shortly show, the following requirement is sufficient:

$$p_k = \frac{1}{N} \quad \text{and} \quad E_k\tau = \frac{2\pi k}{N}. \tag{5}$$

We see that the energy levels are equally spaced, which intuitively is expected as this causes the periodicities in the dynamics to resonate at specific times, enhancing constructive interference. Such an equally spaced energy spectrum is also found for the generation of perfect state transfer [16]. More specifically, we will soon choose $E_k = \gamma k$ where γ has units of energy, and then $\tau = 2\pi/\Delta E$ where $\Delta E = E_{\rm max} - E_{\rm min}$ is the energy gap between the ground and largest

energy in the spectrum. We note here that a relativistic massless free particle, with energy $E = \sqrt{m^2C^4 + c^2p^2}$, and $m = 0$, has a dispersion $E_k \propto p \propto k$, instead of the well-known Schrödinger dispersion of a free particle $E_k \sim k^2$. Hence, the energy spectrum we find in Eq. (5) is essentially relativistic; the consequence of this for search will be discussed later. We also see that the overlaps p_k are k independent. To verify these requirements, insert Eq. (5) in Eq. (4) and then with summation formulas (see Appendix D) we have

$$\frac{\xi}{N}\sum_{k=0}^{N-1}\frac{1}{\xi - \exp(-i2\pi k/N)} = -\frac{\xi^N}{1-\xi^N} = 0 \tag{6}$$

and the only possible solution is $\xi = 0$. We see that for a quantum system satisfying Eq. (5), the survival operator has a N-fold degenerate eigenvalues at $\xi = 0$, as we aimed for. The order of the exceptional point is equal to the size of the Hilbert space N, namely,

$$\xi = 0, \quad N\text{th-order exceptional point.} \tag{7}$$

It can also be shown that Eq. (5) is in fact a necessary condition for a degree N exceptional point (see Appendix E). Further, all the right and left eigenvectors also coalesce with $|\xi^R\rangle = U(\tau)^{-1}|\psi_d\rangle = U(-\tau)|\psi_d\rangle$ and $\langle\xi^L| = \langle\psi_d|$. Before constructing the graph that yields this result, we study its general consequences for search.

III. EFFICIENT QUANTUM SEARCH AND QUANTIZED TOPOLOGICAL WINDING NUMBER

We denote H_s, U_s and $\mathcal{S}_s$ the Hamiltonian, unitary, and survival operator for a system that satisfies the efficient search conditions (5) and in this notation we omit the dependence on τ. We define the states $|Q_k\rangle = (U_s)^k|\psi_d\rangle$ with $k = 0, \ldots, N-1$. The operators U_s and $\mathcal{S}_s$ acting on these states give

$$\begin{aligned} &U_s|Q_{N-1}\rangle = |\psi_d\rangle, \quad U_s|Q_k\rangle = |Q_{k+1}\rangle \text{ if } k \neq N-1, \\ &\mathcal{S}_s|Q_{N-1}\rangle = 0, \quad \mathcal{S}_s|Q_k\rangle = |Q_{k+1}\rangle \text{ if } k \neq N-1. \end{aligned} \tag{8}$$

These formulas are mathematically straightforward, for example, $U_s|Q_{N-1}\rangle = (U_s)^N|\psi_d\rangle = \sum_{k=0}^{N-1}(U_s)^N\langle E_k|\psi_d\rangle|E_k\rangle = \sum_{k=0}^{N-1}\exp(-iE_k\tau N)\langle E_k|\psi_d\rangle|E_k\rangle = |\psi_d\rangle = |Q_0\rangle$ where we used Eq. (5) and hence $\exp(-iE_k\tau N) = 1$. We see that both $\mathcal{S}_s$ and U_s are shift operators, their difference being the action on the boundary term $|Q_{N-1}\rangle$. We can also show that the states $|Q_k\rangle$ are orthonormal $\langle Q_l|Q_m\rangle = \delta_{lm}$ (see Appendix F) and they form a complete set spanning any initial condition in the Hilbert space. From here we reach the following conclusions. First, consider an initial condition which is a $|Q_k\rangle$ state, then following Eq. (1) we consider the operation $(\mathcal{S}_s)^n|Q_k\rangle$ and using Eq. (8) we obtain

$$\phi_n = \begin{cases} 1 & \text{if } n = N-k, \\ 0 & \text{otherwise.} \end{cases} \tag{9}$$

This means that we detect the target with probability one at time $(N-k)\tau$, hence, the detection process is deterministic as the fluctuations of the detection time vanish. Then when $|\psi_0\rangle = |Q_k\rangle$, we have

$$P_{\text{det}} = 1, \quad \langle t\rangle = t = \tau(N-k), \quad \text{Var}(t) = 0. \tag{10}$$

For a more general initial condition, exploiting the fact that the states $|Q_k\rangle$ form a complete set and the linearity of Eq. (1) with respect to the initial condition, the probability of first detection $F_n = |\phi_n|^2$ is

$$F_n = \begin{cases} |\langle Q_{N-n}|\psi_{\text{in}}\rangle|^2 & \text{for } n = 1, \ldots, N, \\ 0 & \text{otherwise.} \end{cases} \tag{11}$$

This implies a guaranteed search since even in the absence of knowledge about the initial condition, the search will find the target with at most N operations. From here it also follows that we have an upper bound on the search time for any initial state

$$t \leqslant \tau N = \frac{2\pi k}{E_k} = \frac{2\pi}{\gamma}. \tag{12}$$

This upper bound is N independent, so the maximum search time does not increase with the system size. The upper limit is found when the initial condition is the target state $|\psi_{\text{in}}\rangle = |\psi_d\rangle$. To conclude, for a quantum walker starting from an unknown initial state, i.e., a black-box problem, our strategy will find this walker at the target state within a fixed time with probability one.

We next explore the topological properties of the efficient quantum search. In spatially periodic systems, such as the topological materials, their topologies are revealed by the Chern number or winding number of the Bloch Hamiltonian in the band-theory framework [48]. For our model, the periodicity originates from the stroboscopic measurements. Hence, instead of a Brillouin zone in k space, here we investigate the topology of the system in the Laplace domain [42]. Using the Z transform, the generating function of the search amplitude ϕ_n reads as

$$\hat{\Phi}(\theta) = \sum_{n=1}^{\infty} e^{in\theta}\phi_n = \frac{\langle\psi_d|\hat{\mathcal{U}}(\theta)|\psi_0\rangle}{1 + \langle\psi_d|\hat{\mathcal{U}}(\theta)|\psi_d\rangle}, \tag{13}$$

where $\hat{\mathcal{U}}(\theta) = \sum_{n=1}^{\infty} e^{in\theta}U(n\tau) = e^{i\theta}U(\tau)/[1 - e^{i\theta}U(\tau)]$ is the generating function of $U(n\tau)$ [43]. The statistics of the search process can be calculated in terms of the generating function. For example, the total search probability $P_{\text{det}} = 1/(2\pi)\int_0^{2\pi} d\theta|\hat{\Phi}(\theta)|^2$ and the mean search time $\langle t\rangle = \tau/(2\pi i)\int_0^{2\pi} d\theta[\hat{\Phi}(\theta)]^*[\partial_\theta\hat{\Phi}(\theta)]$, where $*$ is the complex conjugate of the generating function [42].

With Eq. (13), we calculate the winding number when the quantum system meets the conditions in Eq. (5), corresponding to an Nth-order exceptional point. The winding number is quantized and characterized by the choice of the initial state. When $|\psi_0\rangle = |Q_k\rangle$, the winding number Ω reads as

$$\Omega = \frac{1}{2\pi i}\int_0^{2\pi} d\theta\, \partial_\theta \ln[\hat{\Phi}(\theta)] = N - k. \tag{14}$$

Using Eq. (11), this quantized winding number equals the number of measurement attempts needed to detect the walker with probability unity. It is in this sense that the search process is related to the topology of the model in Laplace space and the search times for states $|Q_k\rangle$ are given in terms of τ multiplied by the number of windings, i.e., $t = \Omega\tau$. We plot $\hat{\Phi}(\theta)$ in Fig. 2 for $N = 3$. Note here we use the crawl Hamiltonian later derived in Eq. (16) for illustration. As shown in the figure, the

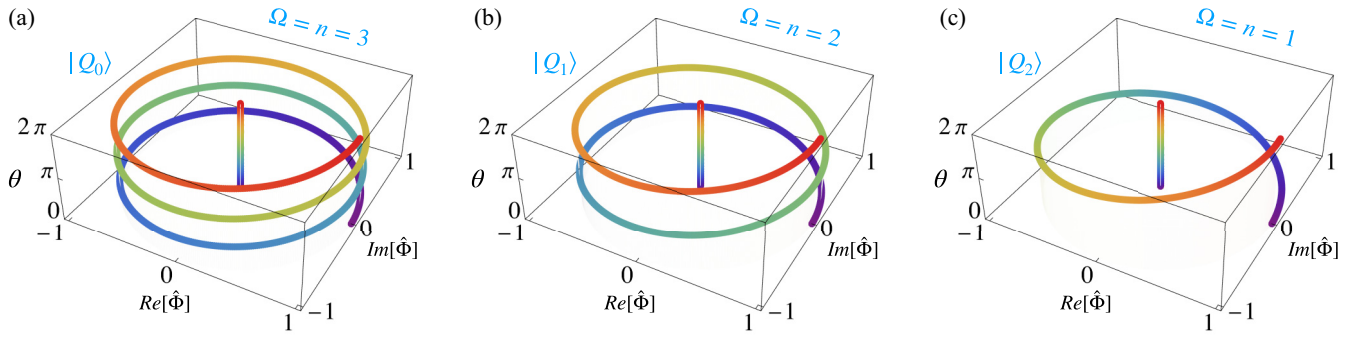

FIG. 2. Topological winding. Plot of the generating function $\hat{\Phi}(\theta)$ versus θ for $N = 3$. Here we choose the crawl Hamiltonian in Eq. (16) and the generating function is given by Eq. (13). The initial states are the three $|Q_k\rangle$s which span the full Hilbert space. Due to the topology of the model, generating function forms a closed circle in the Laplace domain, hence the winding number is quantized as predicted in Eq. (14). As shown in the figure, for the winding number of initial state $|Q_0\rangle$, we have $\Omega = 3$ (a). The winding number of $|Q_1\rangle$ is 2 (b) and the winding number for $|Q_2\rangle$ is 1 (c). These windings give the number of the measurements for the successful search.

$\hat{\Phi}(\theta)$ forms closed circles and the number of times it rotates around the center is equal to Ω.

IV. EXAMPLES OF DESIGNED QUANTUM GRAPHS: CRAWL AND FUNNEL MODELS

What are the tight-binding Hamiltonians of size $N \times N$, that yield a guaranteed search? The condition in Eq. (5) admits many types of solutions, and here we present two that have certain advantages. We will also discuss the connection to perfect state transfer [16].

A. Crawl model

First, we present an approach where the nodes of the graph are the states $|Q_k\rangle$. This is clearly useful since this means that we can start the process with the wave packet on one node of the graph and find the walker with probability one after a fixed time at any other node, which we call deterministic search, as the fluctuations vanish. We use $H = \sum_k E_k |E_k\rangle\langle E_k|$ and for the equally spaced energies we set $E_0 = 0, E_1 = \gamma, \ldots, E_{N-1} = (N-1)\gamma$ and Eq. (5) gives $\tau = 2\pi/N\gamma$. More generally $\tau = 2\pi/N\gamma + 2j\pi/\gamma$ and j is a non-negative integer. In this system the states $|x\rangle$ with $x = 0, 1, \ldots, N-1$ are the nodes of the graph (see Fig. 1). To perform this trick let

$$|E_k\rangle = \left\{1, e^{i\theta_k}, e^{i2\theta_k}, \ldots, e^{i(N-1)\theta_k}\right\}^T/\sqrt{N}, \tag{15}$$

where $\theta_k = 2\pi k/N$. This eigenstate is a discrete Fourier wave, which is related to the "relativistic" linear dispersion in Eq. (5), and Dirac physics as discussed below. Clearly Eq. (15) gives $p_k = 1/N$ and hence

$$H_{\rm crawl} = \gamma \begin{bmatrix} 0 & \frac{1}{1-e^{i\theta_1}} & \frac{1}{1-e^{i\theta_2}} & \cdots & \frac{1}{1-e^{i\theta_{N-1}}} \\ \frac{1}{1-e^{-i\theta_1}} & 0 & \frac{1}{1-e^{i\theta_1}} & \cdots & \frac{1}{1-e^{i\theta_{N-2}}} \\ \frac{1}{1-e^{-i\theta_2}} & \frac{1}{1-e^{-i\theta_1}} & 0 & \cdots & \frac{1}{1-e^{i\theta_{N-3}}} \\ \vdots & \vdots & \vdots & \ddots & \vdots \\ \frac{1}{1-e^{-i\theta_{N-1}}} & \frac{1}{1-e^{-i\theta_{N-2}}} & \frac{1}{1-e^{-i\theta_{N-3}}} & \cdots & 0 \end{bmatrix} \tag{16}$$

which we call the crawl Hamiltonian [see a schematic diagram in Fig. 1(a)]. This system, as discussed below, breaks time-reversal symmetry. Namely, the unidirectional movement of the packet can be reversed by changing $H_{\rm crawl}$ to its complex $H^*_{\rm crawl}$, which is a feature of time reversal. In Fig. 3(a) we plot F_n for a system with $N = 50$ and where the target state is $|\psi_{\rm d}\rangle = |0\rangle$. We choose local initial conditions such that $|\psi_{\rm in}\rangle = |x\rangle$, hence, we are considering a transition from x to 0 and in the plot we choose $x = 0, 1, \ldots, 49$. We see that F_n is sharply peaked and is equal to unity when $n = x$ [Fig. 3(a)]. This type of deterministic search is not found for classical random walks, and relies on the fact that the quantum wave packet can, at specific times of the evolution, be localized on a single node, while at prior measurement times the wave packet vanishes on the node. This $H_{\rm Crawl}$ is very much related to unitary state transfer in the absence of measurements, as discussed below.

Connection to perfect state transfer

Previously, Kostak *et al.* [16] considered the problem of perfect state transfer using the permutation matrix $\mathcal{P}_{\rm pst}$. The basic idea there is to find a class of Hamiltonians, whose unitary evolution in the time interval τ equals a permutation matrix which transfers the first entry of the graph to the last one, i.e., $e^{-iH\tau} = \mathcal{P}_{\rm pst}$. The condition for the permutation matrix is that the last term in the first column of $\mathcal{P}_{\rm pst}$ is one, which transfers the wave packet on the first node to the last node, achieving the perfect quantum state transfer between them. As an example, for a system with four states,

$$\mathcal{P}_{\rm pst} = \begin{bmatrix} 0 & 0 & 0 & 1 \\ 0 & 0 & 1 & 0 \\ 0 & 1 & 0 & 0 \\ 1 & 0 & 0 & 0 \end{bmatrix}. \tag{17}$$

Clearly, this transforms the initial state $|1000\rangle$ (i.e., the entrance node) to the final state $|0001\rangle$ (i.e., the target node) and hence one gets the perfect state transfer between them.

In contrast, we investigate the effects of repeated measurements on the search for an unknown initial state by designing special graphs, using the conditions that generate an exceptional point of the highest possible order. In special cases, the

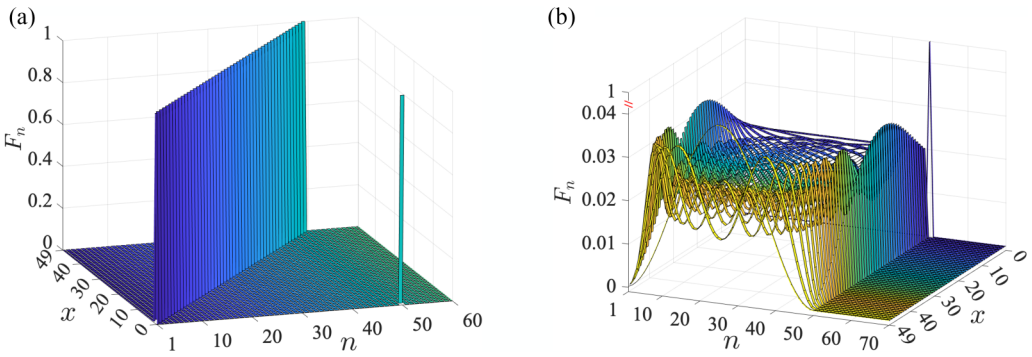

FIG. 3. Guaranteed and fast quantum search. Detection probability F_n versus n for the crawl (a) and funnel (b) models. Here the graph has $N = 50$ nodes and we present results with initial states localized on one of the nodes $|\psi_{\text{in}}\rangle = |x\rangle$, $x = 0, 1, \ldots$ and $|\psi_{\text{d}}\rangle = |0\rangle$ (Appendix B). For the crawl search we find a deterministic outcome of the process, where $F_n = 1$ when $n = x$ (for $x = 0$, $F_{50} = 1$). For the funnel model (b) notice the sharp cutoff of F_n for $n > N = 50$. For any initial condition, the detection of the state is guaranteed with probability one, within at most N measurements, which we call guaranteed search. In (b) notice the peak of height one for $n = 50$, when the initial condition is the same as the detected state. The upper bound for the search time is $t_{\max} = \tau N = 2\pi$.

design we propose here is the same as the one found in [16], even if the protocol of measurement is not the same. To see this special case, consider a walker that starts from the entry node (i.e., the first node) of the crawl graph, in other words, we now assume the complete knowledge of the initial state, which is a special localized state. As mentioned, using the crawl model the unitary $U(\tau)$ is the shift operator, which shifts the particle from one node to the other (see Fig. 6). In other words, the evolution propagator for the crawl model is a specialized permutation matrix [16]. Using Eq. (16), as an example we choose $N = 4$, then the evolution propagator reads as

$$e^{-iH_{\text{crawl}}\tau} = \begin{bmatrix} 0 & 1 & 0 & 0 \\ 0 & 0 & 1 & 0 \\ 0 & 0 & 0 & 1 \\ 1 & 0 & 0 & 0 \end{bmatrix} = \mathcal{P}_{\text{crawl}}. \tag{18}$$

In the paper, Kostak *et al.* denote such matrices as the one-cycle permutation matrix [16], in the sense that all the elements in the matrix rotate in a single permutation cycle. Actually, the one-cycle permutation matrix can achieve perfect state transfer between any nodes in the system by repeatedly utilizing the permutation matrix, for any localized initial condition, namely, $|1000\rangle$, $|0100\rangle$, $|0010\rangle$, and $|0001\rangle$. Since in this example the measurements do not destroy the unitarity until the final measurement, the crawl Hamiltonian is equivalent to quantum state transfer with unitary dynamics. The difference is that we must apply the permutation matrix at most four times to detect the particle from an arbitrary initial condition. In perfect state transfer, on the other hand, one needs to apply either $\mathcal{P}_{\text{pst}}$ or $\mathcal{P}_{\text{crawl}}$ only once, due to the specified initial condition.

However, not all permutation matrices can perform the guaranteed quantum search even with repeated measurements. Actually, all many-cycle permutation matrices [for example, Eq. (17) has two cycles] have a subspace that cannot be transported to the search target. For instance, using the permutation matrix $\mathcal{P}_{\text{pst}}$ given in Eq. (17), only the amplitudes on the first and last nodes can be searched in the target state (node four), while the amplitudes on the second and third nodes never reach the search target. This makes the $P_{\text{det}} < 1$ even after an infinite number of measurements, which would be a fatal flaw in the search problem considered in this work.

On the other hand, most of the Hamiltonians that are given by conditions in Eq. (5) do not correspond to a permutation matrix. This is easy to understand since our approach is based on the high-order exceptional point and non-Hermitian process generated by repeated measurements. As we will soon show, in the next model, called the funnel model H_{funnel}, we have

$$e^{-iH_{\text{funnel}}\tau} = \frac{1}{2}\begin{bmatrix} 0 & \frac{2}{\sqrt{3}} & \frac{1-3i}{\sqrt{6}} & -\frac{1+i}{\sqrt{2}} \\ \frac{2}{\sqrt{3}} & \frac{4}{3} & -\frac{\frac{1}{3}-i}{\sqrt{2}} & \frac{1+i}{\sqrt{6}} \\ \frac{1-3i}{\sqrt{6}} & -\frac{\frac{1}{3}-i}{\sqrt{2}} & -\frac{1}{3}-i & \frac{1+i}{\sqrt{3}} \\ -\frac{1+i}{\sqrt{2}} & \frac{1+i}{\sqrt{6}} & \frac{1+i}{\sqrt{3}} & -1+i \end{bmatrix}. \tag{19}$$

Clearly, the evolution propagator is not a permutation matrix. The state $|1000\rangle$ is not transferred to $|0001\rangle$, in one operation. Each measurement has a finite probability to record the target state, hence, these measurements randomly collapse the target state in the search process. In other words, the combined effect of measurements and unitaries plays a crucial role here. As mentioned, the crawl model breaks time-reversal symmetry, while the funnel model does not, a fact that could have implications in the laboratory when constructing these systems.

B. Funnel model

An alternative approach that uses onsite energies to direct the search to a specific node denoted $|\psi_{\text{d}}\rangle = |0\rangle$ is now considered. Here the process does not break time-reversal symmetry. As before, the spatial nodes of the graph are denoted $|x_i\rangle$, and $i = 0, 1, \ldots, N-1$. We still have condition to fulfill in Eq. (5) and we start with the normalized state $|E_0\rangle = \{1/\sqrt{N}, -\sqrt{N-1}/\sqrt{N}, 0, \ldots\}^T$ in agreement with the second condition in Eq. (5). The next energy state is constructed such that it is normalized and orthogonal to the first one and has an overlap $1/N$ with the detected state $|E_1\rangle = \{1/\sqrt{N}, 1/\sqrt{N(N-1)}, -\sqrt{N-2}/\sqrt{N-1}.0, 0, \ldots\}^T$. The process of constructing these states is then continued (Appendix G), and exploiting the demand that energy levels be

equispaced, Eq. (5), we find

$$H_{\text{funnel}} = \frac{\gamma}{2}\begin{bmatrix} N-1 & \sqrt{N-1} & \cdots & \sqrt{\frac{2}{N}} \\ \sqrt{N-1} & 1 & \cdots & \sqrt{\frac{2}{N^2-N}} \\ \vdots & \vdots & \ddots & \vdots \\ \sqrt{\frac{2}{N}} & \sqrt{\frac{2}{N^2-N}} & \cdots & 2N-3 \end{bmatrix} \quad (20)$$

with matrix elements $H_{0,m}=\sqrt{(N-m)(N-m+1)/N}$ $(m\neq 0)$ and $H_{j,m} = \sqrt{(N-m)(N-m+1)/[(N-j+1)(N-j)]}$ $(j \neq 0, m)$. We call this approach the funnel model. This type of system is schematically shown in Fig. 1(b) while in Fig. 3(b) we present the detection probabilities for localized initial conditions. Figure 3(b) illustrates a sharp cutoff, namely, $F_n = 0$ for any $n > N$ and thus the search is guaranteed to succeed in a finite time, a feature completely absent in classical random walks or quantum walks on nonspecialized graphs. Interestingly, if the initial state is the same as the detected one, corresponding to what is known as the return problem [40], $F_{50} = 1$, otherwise it is zero. This means the system is detected exactly after N attempts, and this feature is universal, namely, for any search H_s, satisfying Eq. (5), and for $|\psi_d\rangle = |\psi_0\rangle$, $F_N = 1$ and $F_{n\neq N} = 0$. We will discuss this surprising effect in more detail in the discussion.

V. COMPARISON TO THE OTHER GRAPHS, INFLUENCE OF NOISE, AND CONNECTIONS TO DIRAC PHYSICS

As a comparison, we calculate the search time for finding the quantum walker on a full randomly connected Sherrington-Kirkpatrick (SK) model [49] with 50 nodes, in the sense that the designed coupling in our model is replaced by the random connections. As we have shown, for our designed graphs with 50 nodes, the walker will be detected within 50 measurement attempts and the upper bound of the search time is $2\pi/\gamma$. As shown in Fig. 4, on the SK model, the mean number of the measurement to find the walker is much larger than our designed graphs ($\langle n\rangle \sim 10^3 \gg 50$) and fluctuates strongly for different choices of τ. When τ is small, the detection times diverge due to the quantum Zeno effect [45,50–52].

We also plot the cases when there is noise on τ in Fig. 5. Here we choose the funnel model with $N = 50$ and the initial state is $|\psi_0\rangle = |49\rangle$. For each sampling interval τ, we use the designed τ [Eq. (5)] with the noise generated from a uniform distribution (see Appendix B). We plot the detection probability versus measurements for different noise strengths. The model shows robustness to the effects of the noise, where the search is still guaranteed to succeed, namely, $\sum_{n=1}^{50} F_n \sim 1$. The detection probability is close to zero for $n > 50$ as shown in Fig. 5. As a more realistic test of the guaranteed search, we calculate the search probability P_{det} within 50 measurements for 1000 realizations. We find $P_{\text{det}} \sim 0.98$ even under 10% noise, hence, the approach is robust.

In comparison with other previous results [53–55], our strategy improves the search process in the following ways: (1) Our search is efficient for any initial state. Previous results have shown that the search is efficient on the graphs like glued trees [53] or hypercubes [55], while this only works for particular initial states. For example, in glued trees, the initial state is one root of the tree and the target is another root of the tree and, in hypercubes, the initial states and target states are opposite corners. For other initial states, the search

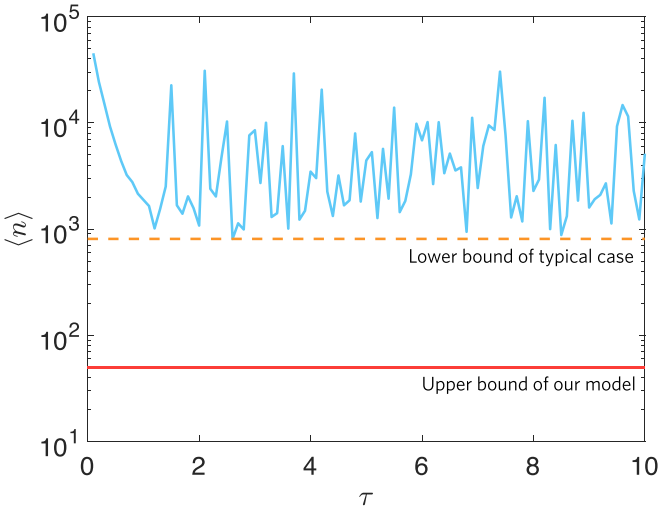

FIG. 4. Comparison with typical graph. We plot the mean measurement numbers for a full randomly connected SK graph for different choices of τ with stroboscopic search protocol. Here we choose $N = 50$ and for the designed graph the upper bound of the measurement number is 50 with time $t \leqslant 2\pi/\gamma$ for $\tau = 2\pi/\Delta E$. The search on the typical graph is much slower than that. As shown in the figure, the lower bound of the SK graph is much bigger that the upper bound of our models. It is clear the designed graphs boost the quantum search process.

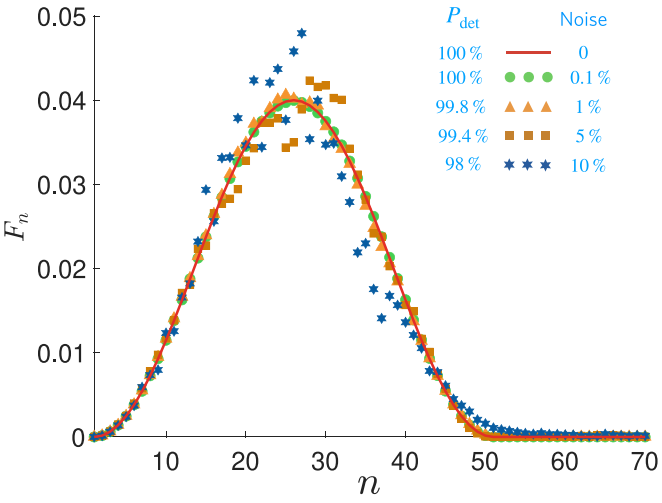

FIG. 5. Noise robustness. We plot the search probability F_n of the 50-site funnel model with the initial state being a node of the graph. We introduce random noise to τ with different magnitudes from 0.1% (green dots) to 10% (blue hexagrams). As shown in the figure, the F_n is robust to the noise and the search probability is nearly zero for $n > 50$. We calculate the total search probability P_{det} within the first 50 measurements for 1000 realizations. The guaranteed search reminds even for comparable large noise, where the $P_{\text{det}} \sim 98\%$ with noise 10%.

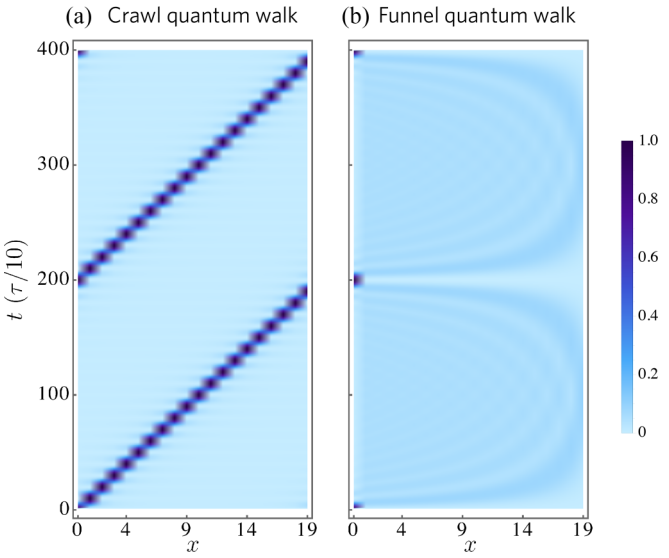

FIG. 6. Nonmonitored quantum walk and perfect quantum state transfer (see also [16]). The time evolution of the wave packet on the crawl (a) and funnel (b) graphs for nonmonitored quantum walks. The color code gives the probability of finding the walker on a node. For the crawl graph, the wave function is fully localized one node after the other at times $\tau, 2\tau, \ldots$, a feature which is vital for state transfer to any node in the system. Both quantum walks exhibit revival, namely, the wave function returns to its initial state, at time $N\tau$.

time can be infinite [54,56]. As a comparison, the search on our designed graph is optimal for any initial states. (2) Our search is guaranteed to succeed even if the size of the system is very large. Previous results have shown that the search probability is high for some measuring times, while in general, the search probability is smaller than one, especially for large systems [53]. In our model, however, the search is guaranteed to succeed with a probability equal to one in a bounded time for any initial states and for any finite size of the system.

The efficient quantum walks we found here are reminiscent of the physics of a massless Dirac particle in dimension one. First, the energy is linear in k [Eq. (5)]. Second, in the crawl model the energy states are discrete free waves and, finally, due to time-reversal breaking, the wave packet can travel either clockwise or anticlockwise, somewhat similar to a particle and antiparticle. But why do we find this relation between our problem and these relativistic effects? We started this work with the demand that the eigenvalues of $\mathcal{S}$ are real and all coalesce to zero to speed up the search process. We then added rotational invariance of the searching process, such that all nodes of the graph are identical, namely, no matter what the detected state, $p_k = 1/N$ on every node of the specially designed graph. We then naturally find the ideal search for a quasiparticle with no dispersion, at least at the measurement times. Namely, a wave packet that is widening will create a less efficient search, in the sense that it renders impossible the absolute detection of the particles in a single measurement made at a node, a feature that is also revealed by the quantized winding number in the Laplace domain. Similarly inspired by a massless Dirac particle, consider the trivial wave equation in continuous space and time in dimension one, $\partial_x \psi(x,t) = \partial_t \psi(x,t)$, the solution is $\psi(x,t) = \int g(k) \exp[i(kx - w_k t)]$ and $g(k)$ is the initial packet in momentum space. For a localized initial condition and using $w = k$, we get a delta traveling wave, in close analogy with what we find in discrete space. Of course, the underlying dynamics in our case is controlled by the Schrödinger equation, but the Hamiltonian under study yields effective motion in which space and time are treated on the same footing. Finally, Dirac's wave function in dimension one has two components. Similarly, we have a particle traveling clockwise and anticlockwise, in fact, at least in principle, we can switch between these modes, if in the middle of the experiment we replace the Hermitian crawl H with its complex conjugate.

VI. DISCUSSION

We have designed a survival operator $\mathcal{S}(\tau)$, with an exceptional point whose degeneracy is the size of the Hilbert space. Such an exceptional point reaches the highest order of degeneracy possible in the model and can be designed as large as possible. This is certainly an advance in exceptional physics compared to previous results [36] considering second- or third-order exceptional points. In general, for an N-dimensional system, to find the highest-order exceptional point, one needs to solve an Nth-order characteristic polynomial [57,58], which, in principle, is difficult when the system is large. Here we show that the high-order exceptional point can be designed by exploiting the symmetry of the model, which leads to the two conditions we discussed in Eq. (5). At the exceptional point, the vector space is severely skewed, as all the eigenstates of $\mathcal{S}(\tau)$ coincide. Obviously, this means that the single eigenstate of $\mathcal{S}(\tau)$ cannot be used to construct a full basis. So can we find a new basis that spans the Hilbert space, which should also be connected to the exceptional properties of the model? This challenge is solved by the states $|Q_k\rangle$ we proposed, which form a full basis that can be used to expand any initial state of the walker, and is determined by the system parameters at the exceptional point. In this new basis, the survival operator $\mathcal{S}(\tau)$ becomes a shift operator (8). Roughly speaking, this new basis can be considered to play the role of the energy eigenbasis found for unitary dynamics. The new basis $|Q_k\rangle$ is an efficient tool for studying the quantum search process. We find a full basis using the exceptional point, which is related to the fact that the degree of the exceptional point here is the size of the Hilbert space, while if the degree of the exceptional point is less than that, the effect would not have been found.

Remarkably, the search probability is sharply peaked, i.e., $F_{n=N} = 1$, for the case $|\psi_{\rm d}\rangle = |\psi_{\rm in}\rangle$, as shown in Fig. 3(b). Since the initial state here is the same as the target one, this is called in the literature the return problem [40]. This is a generic property for all the designed graphs and describes the special recurrence property in repeatedly monitored quantum walks. To see this note that choosing $k = 0$, $|Q_0\rangle = |\psi_{\rm d}\rangle$, and then use Eq. (15). Physically, this shows the wave function always has destructive interference on the search target at times $n\tau$ with $n = 1, \ldots, N-1$ and fully constructive interference, which collects all the amplitude of wave function, at time $N\tau$ at $|\psi_{\rm d}\rangle$. In connection with previous results, Grünbaum *et al.* have shown that the mean search time for the return

problem is quantized and equals the effective dimension of the system [40,59], which is related to the topology of the Schur functions. This result in our case means that the average $\langle n\rangle = N$ for the return problem. However, as shown in our work, for purposely designed graphs, we have $F_n = 0$ for $n > N$ for the guaranteed search. These two results together mean that in our case we must have $F_N = 1$ for the return problem. The result is therefore the sharp peak seen in Fig. 3. This means that in general for the return problem $\mathrm{Var}(n) \neq 0$, while we have $\mathrm{Var}(n) = 0$, namely, no fluctuations at all of the return time. This indicates a specialized recurrence on our designed graphs, which is absent in previous results.

The resulting special purpose family of Hamiltonians allows for guaranteed search. The main condition in Eq. (5) still allows for further freedom in the design of the search process. For specialized states $|Q_i\rangle$, which are used to expand the Hilbert space as we discussed, the monitored search process is deterministic as the fluctuations in the detection attempt vanish. Our work shows a connection between guaranteed search and the topology (see Fig. 2). Very generally, starting with state $|Q_i\rangle$ the generating function winds, the number of windings gives the number of measurements until detection. Hence, the search time can also be expressed in terms of the winding number times τ, i.e., $t = \Omega\tau$. For a random unknown initial state, the quantum walks we designed here are guaranteed to succeed in a bounded time. Usually, topology is related to some protected physical reality that is insensitive to sources of noise. Also in our case, the topology is related to a physically robust result, i.e., protecting the search in the sense that it is secured to be detected, up until a fixed time, no matter what is the initial state.

For the crawl model, the search is effectively unidirectional in a system that conserves energy. The Hamiltonian is independent of the choice of the target state, and in that sense, the system exhibits universal search. The H_{crawl} breaks time-reversal symmetry, and is related to the Dirac equation. In contrast, the funnel model does not break time-reversal symmetry, but the target state is unique.

To conclude, our search is globally optimal with respect to any other search algorithm, in the sense that the success probability is unity within a finite time even for large systems and for all initial conditions.

ACKNOWLEDGMENTS

E.B. thanks S. Yankelevich, M. Goldstein, and L. Khaikovich for comments and suggestions. The support of Israel Science Foundation's Grant No. 1614/21 is acknowledged.

APPENDIX A: MATRIX DETERMINANT LEMMA

We provide details on the derivation of Eq. (2) using the matrix determinant lemma. Suppose A is an invertible square matrix and u, v are column vectors, then the matrix determinant lemma states

$$\det|A + uv^T| = (1 + v^T A^{-1} u)\det|A|, \tag{A1}$$

where uv^T is the outer product of the vectors u and v. We are interested in the eigenvalues of the survival operator $\det|\xi - \mathcal{S}(\tau)| = 0$ with $\mathcal{S}(\tau) = (1 - |\psi_{\mathrm{d}}\rangle\langle\psi_{\mathrm{d}}|)U(\tau)$ as defined in the main text. Substituting $\mathcal{S}$ into the matrix determinant, we have

$$\det|\xi - \mathcal{S}(\tau)| = \det|\xi - U(\tau) + |\psi_{\mathrm{d}}\rangle\langle\psi_{\mathrm{d}}|U(\tau)|. \tag{A2}$$

As discussed in the main text, to prevent the appearance of dark states, which are not optimal for the quantum search, we have conditioned $\det|\xi - U(\tau)| \neq 0$. Hence $\xi - U(\tau)$ is an invertible square matrix. If we denote $\xi - U(\tau)$ as the matrix A, it fits the condition for the matrix determinant lemma. We then let $u = |\psi_{\mathrm{d}}\rangle$, and $v^T = \langle\psi_{\mathrm{d}}|U(\tau)$. Using Eq. (A1), we get Eq. (2) used in the main text.

APPENDIX B: NUMERICAL SIMULATION APPROACH

To prepare the plots, we simulate the search process directly based on Eq. (1). We first construct the search Hamiltonians for the crawl graph and funnel graph using Eqs. (16) and (20). In the simulation, we set $N = 50$ (for preparation of Fig. 3). The initial state of the system is usually a node of the graph, namely, $|\psi_{\mathrm{in}}\rangle = |x\rangle$. We represent it by a vector of dimension N. For example, if the system is initially localized on node 0, we set the first entry of the vector to be one and all the rest remains zero. With the initial state and funnel and crawl Hamiltonians, we numerically calculate ϕ_1, which is the overlap between the wave function at time τ and the search target $|\psi_{\mathrm{d}}\rangle$, namely, $\phi_1 = \langle\psi_{\mathrm{d}}|U(\tau)|\psi_{\mathrm{in}}\rangle$. The square of $|\phi_1|$ is the probability that we detect the particle in the first measurement at time $t = \tau$, which is recorded for plotting Fig. 3. We then turn to the calculation of F_2. In the first step, the failed measurement (at time τ) projects out the state on $|\psi_{\mathrm{d}}\rangle$. This is done by setting the state that overlaps with $|\psi_{\mathrm{d}}\rangle$ to zero, in other words, we mimic the back-action of projection $(1 - |\psi_{\mathrm{d}}\rangle\langle\psi_{\mathrm{d}}|)$. For example, let $|\psi_{\mathrm{d}}\rangle = |0\rangle$, then after the measurement, the state of the system on node 0 is zero. The measured state is the new initial state for the calculation of F_2. Similar to the calculation of F_1, we let the system evolve for time τ by $U(\tau)$, then calculate the overlap between the state of the system and search target, which is ϕ_2. The search probability $F_2 = |\phi_2|^2$. Such procedure is repeated: We numerically calculate $F_3, F_4, \ldots, F_n$. The results are plotted for the crawl in Fig. 3(a) and funnel in 3(b) models. In Fig. 4, we utilize the same process for the calculation of F_n and use the random SK Hamiltonian. The mean measurement times are given by $\langle n\rangle = \sum_{n=1}^{M} nF_n$. In the numerical simulation we choose $M = 100\,000$. In Fig. 5, the time interval between two measurements is random, depending on the magnitude of the noises. For each τ, we choose $\tau = (2\pi/N)\{1 + a * \mathrm{uniform}[-0.5, 0.5]\}$ with a being the magnitude of the noise. For the calculation of the search probability, we use the simulated F_n and sum the first 50 measurements, i.e., $P_{\mathrm{det}} = \sum_{n=1}^{n=N=50} F_n$. For each magnitude of the noise, P_{det} is averaged over 1000 realizations.

APPENDIX C: FIGURE PREPARATION

We now provide further details of the figures.

(i) Figure 1(a). Schematic plot of the crawl graph Hamiltonian in Eq. (16) of size 20×20. Here we set $\gamma = 1$ and subsequently. In Eq. (16), we have a typical matrix element $1/[1 - \exp(i\theta)]$, which can be formally written as $1/[1 -$

$\exp(i\theta)] = R\ \exp(i\Phi)$. The R represents the coupling strength between the nodes, in the figure we utilize the thickness of the connecting line to represent its magnitude. The R decreases as the distance between the nodes becomes longer. For example, $R_{0,1} = R_{0,19} > R_{0,2} = R_{0,18} > R_{0,3} = R_{0,17} > \cdots > R_{0,10}$. The colors represent the phases Φ, where the phases $\pi > \Phi > \pi/2$. The onsite energies of the nodes are equal to zero, hence, all of them are plotted in gray. Geometrically, the system is rotationally invariant.

(ii) Figure 1(b). Schematic plot of the funnel Hamiltonian in Eq. (20) of size 20×20. The matrix elements are real, and again we unitize the thickness of the line connecting the nodes to represent the hopping rate magnitude. Now the onsite energies are not identical, and we present this variation by the colors. The detection node is specialized for this model, and we mark this node in the graph. The onsite energies increase linearly for the nodes from 1 to $N-1$, and for the search node, the onsite energy is approximately $N/2$.

(iii) Figure 3(a). Search probability F_n versus measurement steps n for the crawl graph. Here the graph has 50 nodes. We choose the initial states to be the nodes of the graph, namely, $|\psi_{\rm in}\rangle = |0\rangle, |1\rangle, \ldots, |49\rangle$. As we discussed in the main text, the search state can be any node of the graph, but here for demonstration, we choose $|\psi_{\rm d}\rangle = |0\rangle$. We numerically simulate the search process with the method we discussed above. As shown in the figure, the search is deterministic, namely, we detect the walker with probability one at some specified times, as described in the text.

(iv) Figure 3(b). Search probability F_n versus measurement steps n for the funnel model. Here we set $N = 50$ and the search target is $|\psi_{\rm d}\rangle = |0\rangle$. Again, we choose the initial state to be a node of the graph and x goes from 0 to 49. We then apply the simulation approach discussed above, which gives the statistics of F_n as shown in the figure. For any initial state, the detection of the state is guaranteed with probability one within N measurements. There is a clear cutoff for F_n when $n > N$, which drops to zero, namely, $F_{n>N} = 0$. The upper bound of the search time is found when $|\psi_{\rm in}\rangle = |0\rangle = |\psi_{\rm d}\rangle$, where $F_{50} = 1$ and $F_{n\neq 50} = 0$, and in this case the detection time is 2π.

(v) Figure 6 describes the unitary evolution without measurements (nonmonitored quantum walks) for the crawl Hamiltonian [Fig. 6(a)] and funnel model [Fig. 6(b)]. We plot the probability of finding the walker on node x, $|\langle\psi(t)|x\rangle|^2$ versus x, and for continuous time t (in the unit $\tau/10$). Here, for both graphs, we choose $N = 20$ and the initial state is $|0\rangle$. We record $|\langle\psi(t)|x\rangle|^2$ for all the nodes with sampling time interval $\tau/10$. As shown in the figure, the wave function of the crawl graph is localized at specific nodes of the graph at times $\tau, 2\tau, 3\tau, \ldots$. In the funnel mode [Fig. 6(b)], starting for a localized state $|0\rangle$, the wave function first spreads to the whole graph. Then it returns to the localized state $|0\rangle$. The system is recurrent, which is rooted in the periodicity of the energy spectrum we design.

APPENDIX D: DETAILS ON THE DERIVATION OF EQ. (6)

We present the derivation of Eq. (6). As discussed in the main text, the eigenfunction of the survival operator $\mathcal{S}(\tau)$ can be written as $\xi \sum_{k=0}^{N-1} p_k/[\xi - \exp(-iE_k\tau)] = 0$. Here, we denote the summation as I. With Eq. (5), we have

$$I = \frac{\xi}{N}\sum_{k=0}^{N-1}\frac{1}{\xi - \exp(-i2\pi k/N)} = -\frac{\xi}{N}\sum_{k=0}^{N-1}\frac{\exp(i2\pi k/N)}{1-\xi\ \exp(i2\pi k/N)}, \tag{D1}$$

where we multiply both the numerator and denominator by $\exp(-i2\pi k/N)$ for each term in the summation. We first Taylor expand $1/[1-\xi\ \exp(i2\pi k/N)]$ and get

$$I = -\frac{\xi}{N}\sum_{k=0}^{N-1}\exp(i2\pi k/N)\sum_{j=0}^{\infty}[\xi\ \exp(i2\pi k/N)]^j = -\frac{\xi}{N}\sum_{k=0}^{N-1}\sum_{j=0}^{\infty}\xi^j\exp[i2\pi k(j+1)/N]. \tag{D2}$$

We then calculate I by changing the order of the summations. Namely, we first perform the summation over k, which is a geometric progression with common ratio $\exp[i2\pi(j+1)/N]$. By calculating the geometric progression, we have

$$I = -\frac{\xi}{N}\sum_{j=0}^{\infty}\xi^j\sum_{k=0}^{N-1}\exp[i2\pi k(j+1)/N] = \frac{\xi}{N}\sum_{j=0}^{\infty}\xi^j\frac{1-\exp(i2\pi j)}{1-\exp[i2\pi(j+1)/N]}. \tag{D3}$$

Since j is an integer, the numerator $1-\exp(i2\pi j)$ always equals to zero. The whole fraction is nonzero only when the denominator $1-\exp[i2\pi(j+1)/N]$ also equals to zero. That is possible and happens when $\exp[i2\pi(j+1)/N] = 1$, namely, $j = nN-1$, where n is an integer and goes from 1 to infinity (if n starts from 0, $j=-1$, which goes beyond the regime of j). We replace the summation index j with n, where n goes from 1 to infinity. Then for the summation I, we have

$$I = \frac{\xi}{N}\sum_{j=nN-1}\xi^j N = \frac{\xi}{N}\sum_{n=1}^{\infty}\xi^{nN-1}N = \sum_{n=1}^{\infty}\xi^{nN} = -\frac{\xi^N}{1-\xi^N}. \tag{D4}$$

These are the details of the derivation of Eq. (6) in the main text.

APPENDIX E: NECESSARY CONDITION FOR THE Nth-ORDER EXCEPTIONAL POINT

In this Appendix, we will show Eq. (5) derived in the main text is a necessary condition for the Nth-order exceptional point. For following Eq. (3) in the main text, the eigenvalue function for ξ reads as

$$\mathcal{F}(\xi) = \langle\psi_{\rm d}|\frac{1}{\xi - U(\tau)}|\psi_{\rm d}\rangle = \sum_{k=0}^{N-1}\frac{p_k}{\xi - e^{-iE_k\tau}} = 0. \tag{E1}$$

We now prove Eq. (5) in the main text is the only solution to have a degeneracy of $N-1$ for $\xi_0 = 0$. Namely, this equation is a necessary condition for the high-order exceptional

point we derived. Mathematically, when $\xi_0 = 0$ is $N-1$ degenerate, we have

$$\mathcal{F}(\xi_0) = 0, \quad \mathcal{F}'(\xi_0) = 0, \quad \mathcal{F}''(\xi_0) = 0,$$
$$\mathcal{F}^{(3)}(\xi_0) = 0, \ \ldots, \ \mathcal{F}^{(N-2)}(\xi_0) = 0, \tag{E2}$$

where the indices $'$, $''$, and (3) denote the first-, second-, and third-order derivatives. These conditions lead to $N-1$ equations for the p_k, E_k, and τ. Since $p_k = |\langle E_k|\psi_d\rangle|^2$, we also have the conditions for the form of the p_k, where

$$\sum p_k = 1, \quad \forall\, k,\ p_k \text{ is real and positive.} \tag{E3}$$

Equations (E2) and (E3) ensure Eq. (5) derived in the main text is a necessary condition for the exceptional point. To see that, let us start with the simple case when $N = 2$. Using Eqs. (E2) and (E3), the function for the p_1 and p_2 is

$$p_1 e^{iE_1\tau} + (1-p_1)e^{iE_2\tau} = 0 \ \longrightarrow \ p_1 = \frac{e^{iE_2\tau}}{e^{iE_2\tau} - e^{iE_1\tau}} = \frac{e^{i\Delta_{21}}}{e^{i\Delta_{21}} - 1},$$
$$p_2 = 1 - p_1. \tag{E4}$$

Here we define the energy difference times τ as Δ_{21}, i.e., $(E_2 - E_1)\tau = \Delta_{21}$. Since p_1 is real and finite [Eq. (E3)], we have $e^{i\Delta_{21}} = -1$ in the complex plane. This gives the conditions for the energy spectrum, i.e., $\Delta_{21} = (E_2 - E_1)\tau = \pi + 2k\pi$, $k \in Z$. Namely, the phase between $E_2\tau$ and $E_1\tau$ is π, as given in Eq. (5). Put the energy spectrum back into Eq. (E4), we have $p_1 = \frac{1}{2}$ and $p_2 = \frac{1}{2}$, the equal magnitude as we presented in the main text. So for the $N = 2$ case, the only solution for the degenerate exceptional point is when $p_1 = p_2 = \frac{1}{2}$ and $(E_2 - E_1)\tau = \pi + 2k\pi$.

Similarly, for $N = 3$, we have

$$\begin{cases} p_1 e^{iE_1\tau} + p_2 e^{iE_2\tau} + (1-p_1-p_2)e^{iE_3\tau} = 0, \\ p_1 e^{2iE_1\tau} + p_2 e^{2iE_2\tau} + (1-p_1-p_2)e^{2iE_3\tau} = 0 \end{cases} \rightarrow p_1 = \frac{e^{i(\Delta_{21}+\Delta_{31})}}{(-1+e^{i\Delta_{21}})(-1+e^{i\Delta_{31}})}, \quad p_2 = \frac{e^{i\Delta_{31}}}{(e^{i\Delta_{21}}-1)(e^{i\Delta_{31}}-e^{i\Delta_{21}})}. \tag{E5}$$

Here $\Delta_{21} = (E_2 - E_1)\tau$ and $\Delta_{31} = (E_3 - E_1)\tau$. Using the conditions in Eq. (E3), we have

$$\Delta_{21} = \frac{2\pi}{3} + 2k_1\pi, \quad \Delta_{31} = \frac{4\pi}{3} + 2k_2\pi, \quad k_1, k_2 \in Z. \tag{E6}$$

This is the energy spectrum condition we have in the main text. For the magnitude of the p, substituting Eq. (E6) back into Eq. (E5), we have $p_1 = p_2 = p_3 = \frac{1}{3}$.

So in general, for the N-dimensional system, using Eqs. (E2) and (E3), we have

$$p_1 = \frac{e^{i\sum_{i=2}^{N}\Delta_{i1}}}{\Pi_{i=2}^{N}(e^{i\Delta_{i1}}-1)},$$
$$p_2 = \frac{e^{i\sum_{i=3}^{N}\Delta_{i1}}}{(e^{i\Delta_{21}}-1)\Pi_{i=3}^{N}(e^{i\Delta_{i1}}-e^{i\Delta_{31}})}, \ \ldots,$$
$$p_k = \frac{e^{i\sum_{i=2,i\neq k}^{N}\Delta_{i1}}}{(e^{i\Delta_{k1}}-1)\Pi_{i=2,i\neq k}^{N}(e^{i\Delta_{i1}}-e^{i\Delta_{k1}})}. \tag{E7}$$

Since these p_k should be real and possible, we have the conditions for the Δ_{i1}. This process leads to the energy spectrum conditions as presented in Eq. (5). Substituting the energy level conditions back into Eq. (E7). The corresponding magnitude of the p_k are all equal, i.e., $p_k = 1/N$. To conclude, Eq. (5) is a necessary condition for achieving an Nth-order exceptional point.

APPENDIX F: PROOF OF THE ORTHOGONAL OF STATES $|Q_k\rangle$

We present the proof that the states $|Q_0\rangle, |Q_1\rangle, |Q_2\rangle, \ldots, |Q_{N-1}\rangle$ are orthogonal with each other, namely, $\langle Q_l|Q_m\rangle = \delta_{lm}$. The state $|Q_k\rangle$ is defined by the unitary evolution operator U_s to the power k times the search target $|\psi_d\rangle$, where $U_s = \exp(-iH_s\tau)$ and H_s are search Hamiltonian. To show the orthogonality, we first expanded $|\psi_d\rangle$ in the energy basis, which leads to

$$|Q_m\rangle = (U_s)^m|\psi_d\rangle = \sum_{k=0}^{N-1}(U_s)^m\langle E_k|\psi_d\rangle|E_k\rangle = \sum_{k=0}^{N-1}\exp(-imE_k\tau)\langle E_k|\psi_d\rangle|E_k\rangle = \sum_{k=0}^{N-1}\exp(-i2\pi km/N)\langle E_k|\psi_d\rangle|E_k\rangle. \tag{F1}$$

Here we have used the fact $E_k\tau = 2\pi k/N$. Similarly, we can find the representation of the state $|Q_l\rangle$ in the energy basis. We then calculate the overlap between the states $|Q_m\rangle$ and $|Q_l\rangle$. We have

$$\langle Q_l|Q_m\rangle = \sum_{k=0}^{N-1}\sum_{k'=0}^{N-1}\langle E_k|\langle\psi_d|E_k\rangle \times \exp[i2\pi(kl - k'm)/N]\langle E_{k'}|\psi_d\rangle|E_{k'}\rangle = \sum_{k=0}^{N-1}|\langle\psi_d|E_k\rangle|^2\exp[i2\pi k(l-m)/N]. \tag{F2}$$

The square of the overlap between the detected state $|\psi_d\rangle$ and the energy state $|E_k\rangle$ is denoted as p_k in the main text, namely, $p_k = |\langle\psi_d|E_k\rangle|^2$. Equation (5) states this value is a dependent of k for the search Hamiltonian H_s, where $p_k = 1/N$. So for Eq. (F2), we only need to calculate the summation of $\exp[i2\pi k(l-m)/N]$ from $k = 0$ to $N-1$. This has been done also in Eq. (D3), where $(j+1)$ in Eq. (D3) is replaced by

$(l-m)$ here. We then have

$$\langle Q_l|Q_m\rangle = \frac{1}{N}\sum_{k=0}^{N-1}\exp[i2\pi k(l-m)/N] = \frac{1}{N}\frac{\exp[i2\pi(l-m)]-1}{\exp[i2\pi(l-m)/N]-1}. \quad \text{(F3)}$$

$\langle Q_l|Q_m\rangle$ is nonzero only when $l-m=0, N, 2N, \ldots$. Here $N-1\geqslant l\geqslant 0$ and $N-1\geqslant m\geqslant 0$. Hence, only when $l=m$ we have $\langle Q_l|Q_m\rangle=1$, otherwise $\langle Q_l|Q_m\rangle=0$. Namely, $\langle Q_l|Q_m\rangle=\delta_{lm}$. This is the conclusion we used in the main text. Another thing to notice is that, since the $|Q_k\rangle$ are generated by the unitary operators, it is naturally normalized. Hence, the states $\{|Q_0\rangle, |Q_1\rangle, |Q_2\rangle, \ldots, |Q_{N-1}\rangle\}$ forms a complete and normalized space.

APPENDIX G: FUNNEL MODEL HAMILTONIAN

We provide details on the funnel Hamiltonian and its explicit presentation. In this model, the search target $|\psi_d\rangle=|0\rangle$. As before, the spatial nodes of the graph are denoted $|x_i\rangle$, and $i=0,1,\ldots,N-1$. We start with the energy state $|E_0\rangle=\{1/\sqrt{N}, -\sqrt{(N-1)/N}, 0, 0, \ldots\}$, where $1/\sqrt{N}$ fulfills the first condition in Eq. (5) and $-\sqrt{(N-1)/N}$ stands for normalization. We then construct the energy state $|E_1\rangle$. It should be orthogonal with $|E_0\rangle$ and in agreement with the condition in Eq. (5). We find $|E_1\rangle=\{1/\sqrt{N}, 1/\sqrt{N(N-1)}, -\sqrt{(N-2)/(N-1)}, 0, 0, \ldots\}$. Again, the first term in $|E_1\rangle$ leads to $|\langle E_1|0\rangle|^2=1/N$. The second entry guarantees $\langle E_0|E_1\rangle=0$, and the third entry is for normalization. Following the construction procedure, we have $|E_2\rangle=\{1/\sqrt{N}, 1/\sqrt{N(N-1)}, 1/\sqrt{(N-2)(N-1)}, -\sqrt{(N-3)/(N-2)}, 0, 0, \ldots\}$, and in general $|E_{i\neq N-1}\rangle=\{1/\sqrt{N}, 1/\sqrt{N(N-1)}, \ldots, 1/\sqrt{(N+2-k)(N+1-k)}, \ldots, -\sqrt{(N-1-i)/(N-i)}, 0, 0, \ldots\}$, where k is the index for the kth entry and $2\leqslant k\leqslant i$. This general representation $|E_i\rangle$ can help us construct the states $|E_0\rangle, |E_1\rangle, \ldots, |E_{N-2}\rangle$, but not $|E_{N-1}\rangle$. Let us explain this and then show how to construct $|E_{N-1}\rangle$. When $i=N-2$, we have $|E_{N-2}\rangle=\{1/\sqrt{N}, 1/\sqrt{N(N-1)}, \ldots, 1/\sqrt{6}, -1/\sqrt{2}\}$. Now we cannot utilize the procedure we did before to construct $|E_{N-1}\rangle$ since, roughly speaking, there is no additional space for the normalization. So how to construct the last energy state? We notice the last term in $|E_{N-2}\rangle$ is $-1/\sqrt{2}$, which is special. Let us consider a state where the first $N-1$ terms are the same as those in $|E_{N-2}\rangle$, and the only different one is the last term, where we change the $-1/\sqrt{2}$ to $1/\sqrt{2}$. We can see such a state is orthogonal with $|E_{N-2}\rangle$ and also normalized. This is the last energy state, i.e., $|E_{N-1}\rangle=\{1/\sqrt{N}, 1/\sqrt{N(N-1)}, \ldots, 1/\sqrt{6}, 1/\sqrt{2}\}$. It is also easy to show that this state is orthogonal with respect to the other state, $|E_{N-3}\rangle, |E_{N-4}\rangle, \ldots, |E_0\rangle$. We then have N orthogonal and normalized states fulfill the conditions in Eq. (5).

For the equal distance energies, we set $E_0=0, E_1=\gamma, E_2=2\gamma, \ldots, E_{N-1}=(N-1)\gamma$, the resulting Hamiltonian is

$$H=\frac{\gamma}{2}\begin{bmatrix} N-1 & H_{0,1} & H_{0,2} & \cdots & H_{0,N-1} \\ H_{0,1} & 1 & H_{1,2} & \cdots & H_{1,N-1} \\ H_{0,2} & H_{1,2} & 3 & \cdots & H_{2,N-1} \\ \vdots & \vdots & \vdots & \ddots & \vdots \\ H_{0,N-1} & H_{1,N-1} & H_{2,N-1} & \cdots & 2N-3 \end{bmatrix}, \quad \text{(G1)}$$

where $H_{0,m}=\sqrt{(N-m)(N-m+1)/N}$ $(m\neq 0)$ and $H_{j,m}=\sqrt{(N-m)(N-m+1)/[(N-j+1)(N-j)]}$ $(j\neq 0, m)$. We call this approach the funnel model.

[1] Y. Aharonov, L. Davidovich, and N. Zagury, Quantum random walks, Phys. Rev. A **48**, 1687 (1993).

[2] O. Mülken and A. Blumen, Continuous-time quantum walks: Models for coherent transport on complex networks, Phys. Rep. **502**, 37 (2011).

[3] J. Kempe, Quantum random walks: An introductory overview, Contemp. Phys. **44**, 307 (2003).

[4] A. Ambainis, Quantum walks and their algorithmic applications, Int. J. Quantum Inf. **01**, 507 (2003).

[5] X. Qiang, T. Loke, A. Montanaro, K. Aungskunsiri, X. Zhou, J. L. O'Brien, J. B. Wang, and J. C. F. Matthews, Efficient quantum walk on a quantum processor, Nat. Commun. **7**, 11511 (2016).

[6] A. M. Childs, Universal Computation by Quantum Walk, Phys. Rev. Lett. **102**, 180501 (2009).

[7] A. M. Childs, D. Gosset, and Z. Webb, Universal computation by multiparticle quantum walk, Science **339**, 791 (2013).

[8] X.-Y. Xu, X.-W. Wang, D.-Y. Chen, C. M. Smith, and X.-M. Jin, Quantum transport in fractal networks, Nat. Photonics **15**, 703 (2021).

[9] J. Cao, R. J. Cogdell, D. F. Coker, H.-G. Duan, J. Hauer, U. Kleinekathöfer, T. L. C. Jansen, T. Mančal, R. J. D. Miller, J. P. Ogilvie, V. I. Prokhorenko, T. Renger, H.-S. Tan, R. Tempelaar, M. Thorwart, E. Thyrhaug, S. Westenhoff, and D. Zigmantas, Quantum biology revisited, Sci. Adv. **6**, eaaz4888 (2020).

[10] N. Dudhe, P. K. Sahoo, and C. Benjamin, Testing quantum speedups in exciton transport through a photosynthetic complex using quantum stochastic walks, Phys. Chem. Chem. Phys. **24**, 2601 (2022).

[11] A. M. Childs and J. Goldstone, Spatial search by quantum walk, Phys. Rev. A **70**, 022314 (2004).

[12] H. Tang, C. Di Franco, Z.-Y. Shi, T.-S. He, Z. Feng, J. Gao, K. Sun, Z.-M. Li, Z.-Q. Jiao, T.-Y. Wang, M. S. Kim, and X.-M. Jin, Experimental quantum fast hitting on hexagonal graphs, Nat. Photonics **12**, 754 (2018).

[13] J. I. Cirac, P. Zoller, H. J. Kimble, and H. Mabuchi, Quantum State Transfer and Entanglement Distribution among Distant Nodes in a Quantum Network, Phys. Rev. Lett. **78**, 3221 (1997).

[14] A. Reiserer and G. Rempe, Cavity-based quantum networks with single atoms and optical photons, Rev. Mod. Phys. **87**, 1379 (2015).

[15] S. Chakraborty, L. Novo, A. Ambainis, and Y. Omar, Spatial Search by Quantum Walk is Optimal for Almost all Graphs, Phys. Rev. Lett. **116**, 100501 (2016).

[16] V. Kostak, G. M. Nikolopoulos, and I. Jex, Perfect state transfer in networks of arbitrary topology and coupling configuration, Phys. Rev. A **75**, 042319 (2007).

[17] A. J. Daley, I. Bloch, C. Kokail, S. Flannigan, N. Pearson, M. Troyer, and P. Zoller, Practical quantum advantage in quantum simulation, Nature (London) **607**, 667 (2022).

[18] M. Gong, S. Wang, C. Zha, M.-C. Chen, H.-L. Huang, Y. Wu, Q. Zhu, Y. Zhao, S. Li, S. Guo *et al.*, Quantum walks on a programmable two-dimensional 62-qubit superconducting processor, Science **372**, 948 (2021).

[19] S. Mittal, J. Fan, S. Faez, A. Migdall, J. M. Taylor, and M. Hafezi, Topologically Robust Transport of Photons in a Synthetic Gauge Field, Phys. Rev. Lett. **113**, 087403 (2014).

[20] R. Keil, C. Poli, M. Heinrich, J. Arkinstall, G. Weihs, H. Schomerus, and A. Szameit, Universal Sign Control of Coupling in Tight-Binding Lattices, Phys. Rev. Lett. **116**, 213901 (2016).

[21] F. Caruso, A. Crespi, A. G. Ciriolo, F. Sciarrino, and R. Osellame, Fast escape of a quantum walker from an integrated photonic maze, Nat. Commun. **7**, 11682 (2016).

[22] O. Boada, L. Novo, F. Sciarrino, and Y. Omar, Quantum walks in synthetic gauge fields with three-dimensional integrated photonics, Phys. Rev. A **95**, 013830 (2017).

[23] S. Mittal, V. V. Orre, G. Zhu, M. A. Gorlach, A. Poddubny, and M. Hafezi, Photonic quadrupole topological phases, Nat. Photonics **13**, 692 (2019).

[24] Y. Chen, X. Chen, X. Ren, M. Gong, and G. C. Guo, Tight-binding model in optical waveguides: Design principle and transferability for simulation of complex photonics networks, Phys. Rev. A **104**, 023501 (2021).

[25] T. Manovitz, Y. Shapira, N. Akerman, A. Stern, and R. Ozeri, Quantum simulations with complex geometries and synthetic gauge fields in a trapped ion chain, PRX Quantum **1**, 020303 (2020).

[26] C. Monroe, W. C. Campbell, L.-M. Duan, Z.-X. Gong, A. V. Gorshkov, P. W. Hess, R. Islam, K. Kim, N. M. Linke, G. Pagano, P. Richerme, C. Senko, and N. Y. Yao, Programmable quantum simulations of spin systems with trapped ions, Rev. Mod. Phys. **93**, 025001 (2021).

[27] A. Periwal, E. S. Cooper, P. Kunkel, F. W. Julian, J. D. Emily, and S. S. Monika, Programmable interactions and emergent geometry in an array of atom clouds, Nature (London) **600**, 630 (2021).

[28] D. Bluvstein, H. Levine, G. Semeghini, T. T. Wang, S. Ebadi, M. Kalinowski, A. Keesling, N. Maskara, H. Pichler, M. Greiner, V. Vuletić, and M. D. Lukin, A quantum processor based on coherent transport of entangled atom arrays, Nature (London) **604**, 451 (2022).

[29] M. A. Miri and A. Alù, Exceptional points in optics and photonics, Science **363**, eaar7709 (2019).

[30] M. Liertzer, L. Ge, A. Cerjan, A. D. Stone, H. E. Türeci, and S. Rotter, Pump-Induced Exceptional Points in Lasers, Phys. Rev. Lett. **108**, 173901 (2012).

[31] J. Doppler, A. A. Mailybaev, J. Böhm, U. Kuhl, A. Girschik, F. Libisch, T. J. Milburn, P. Rabl, N. Moiseyev, and S. Rotter, Dynamically encircling an exceptional point for asymmetric mode switching, Nature (London) **537**, 76 (2016).

[32] H. Xu, D. Mason, L. Jiang, and J. G. E. Harris, Topological energy transfer in an optomechanical system with exceptional points, Nature (London) **537**, 80 (2016).

[33] T. E. Lee, Anomalous Edge State in a Non-Hermitian Lattice, Phys. Rev. Lett. **116**, 133903 (2016).

[34] D. Leykam, K. Y. Bliokh, C. Huang, Y. D. Chong, and F. Nori, Edge Modes, Degeneracies, and Topological Numbers in Non-Hermitian Systems, Phys. Rev. Lett. **118**, 040401 (2017).

[35] H. Shen, B. Zhen, and L. Fu, Topological Band Theory for Non-Hermitian Hamiltonians, Phys. Rev. Lett. **120**, 146402 (2018).

[36] E. J. Bergholtz, J. C. Budich, and F. K. Kunst, Exceptional topology of non-Hermitian systems, Rev. Mod. Phys. **93**, 015005 (2021).

[37] A. Guo, G. J. Salamo, D. Duchesne, R. Morandotti, M. Volatier-Ravat, V. Aimez, G. A. Siviloglou, and D. N. Christodoulides, Observation of $\mathcal{PT}$-Symmetry Breaking in Complex Optical Potentials, Phys. Rev. Lett. **103**, 093902 (2009).

[38] R. El-Ganainy, K. G. Makris, M. Khajavikhan, Z. H. Musslimani, S. Rotter, and D. N. Christodoulides, Non-Hermitian physics and PT symmetry, Nat. Phys. **14**, 11 (2018).

[39] L. Xiao, T. Deng, K. Wang, Z. Wang, W. Yi, and P. Xue, Observation of Non-Bloch Parity-Time Symmetry and Exceptional Points, Phys. Rev. Lett. **126**, 230402 (2021).

[40] F. A. Grünbaum, L. Velázquez, A. H. Werner, and R. F. Werner, Recurrence for discrete time unitary evolutions, Commun. Math. Phys. **320**, 543 (2013).

[41] S. Dhar, S. Dasgupta, A. Dhar, and D. Sen, Detection of a quantum particle on a lattice under repeated projective measurements, Phys. Rev. A **91**, 062115 (2015).

[42] H. Friedman, D. A. Kessler, and E. Barkai, Quantum walks: The first detected passage time problem, Phys. Rev. E **95**, 032141 (2017).

[43] F. Thiel, E. Barkai, and D. A. Kessler, First Detected Arrival of a Quantum Walker on an Infinite Line, Phys. Rev. Lett. **120**, 040502 (2018).

[44] Q. Liu, K. Ziegler, D. A. Kessler, and E. Barkai, Driving quantum systems with periodic conditional measurements, Phys. Rev. Res. **4**, 023129 (2022).

[45] V. Dubey, C. Bernardin, and A. Dhar, Quantum dynamics under continuous projective measurements: Non-Hermitian description and the continuum-space limit, Phys. Rev. A **103**, 032221 (2021).

[46] H. Krovi and T. A. Brun, Hitting time for quantum walks on the hypercube, Phys. Rev. A **73**, 032341 (2006).

[47] F. Thiel, I. Mualem, D. Meidan, E. Barkai, and D. A. Kessler, Dark states of quantum search cause imperfect detection, Phys. Rev. Res. **2**, 043107 (2020).

[48] C.-K. Chiu, J. C. Y. Teo, A. P. Schnyder, and S. Ryu, Classification of topological quantum matter with symmetries, Rev. Mod. Phys. **88**, 035005 (2016).

[49] M. P. Harrigan, K. J. Sung, M. Neeley, K. J. Satzinger, F. Arute, K. Arya, J. Atalaya, J. C. Bardin, R. Barends, S. Boixo *et al.*, Quantum approximate optimization of non-planar graph problems on a planar superconducting processor, Nat. Phys. **17**, 332 (2021).

[50] B. Misra and E. C. G. Sudarshan, The zeno's paradox in quantum theory, J. Math. Phys. **18**, 756 (1977).

[51] W. M. Itano, D. J. Heinzen, J. J. Bollinger, and D. J. Wineland, Quantum zeno effect, Phys. Rev. A **41**, 2295 (1990).

[52] P. Facchi, H. Nakazato, and S. Pascazio, From the Quantum Zeno to the Inverse Quantum Zeno Effect, Phys. Rev. Lett. **86**, 2699 (2001).

[53] A. M. Childs, R. Cleve, E. Deotto, E. Farhi, S. Gutmann, and D. A. Spielman, Exponential algorithmic speedup by a quantum walk, in *Proceedings of the Thirty-Fifth Annual ACM Symposium on Theory of Computing*, STOC '03 (Association for Computing Machinery, New York, 2003), pp. 59–68.

[54] H. Krovi and T. A. Brun, Quantum walks on quotient graphs, Phys. Rev. A **75**, 062332 (2007).

[55] J. Kempe, Discrete quantum walks hit exponentially faster, Probab. Theory Relat. Fields **133**, 215 (2005).

[56] Hari Krovi and Todd A. Brun, Quantum walks with infinite hitting times, Phys. Rev. A **74**, 042334 (2006).

[57] Z. Xiao, H. Li, T. Kottos, and A. Alù, Enhanced Sensing and Nondegraded Thermal Noise Performance Based on $\mathcal{PT}$-Symmetric Electronic Circuits with a Sixth-Order Exceptional Point, Phys. Rev. Lett. **123**, 213901 (2019).

[58] H. Hodaei, A. U. Hassan, S. Wittek, H. Garcia-Gracia, R. El-Ganainy, D. N. Christodoulides, and M. Khajavikhan, Enhanced sensitivity at higher-order exceptional points, Nature (London) **548**, 187 (2017).

[59] J. Bourgain, F. A. Grünbaum, L. Velázquez, and J. Wilkening, Quantum recurrence of a subspace and operator-valued schur functions, Commun. Math. Phys. **329**, 1031 (2014).